CHEMISTRY
A European Journal

A Journal of
ChemPubSoc Europe

Accepted Article

Title: Thermodynamic Programming of Erbium(III) Coordination Complexes for Dual Visible-Near Infrared Luminescence

Authors: Claude Piguet, Bahman Golesorkhi, Laure Guénée, Homayoun Nozary, Alexandre Fürstenberg, Yan Suffren, Svetlana Eliseeva, Stéphane Petoud, and Andreas Hauser

To be cited as: *Chem. Eur. J.* 10.1002/chem.201802277

Link to VoR: http://dx.doi.org/10.1002/chem.201802277

Supported by
ACES

WILEY-VCH

Thermodynamic Programming of Erbium(III) Coordination Complexes for Dual Visible-Near Infrared Luminescence

---

Bahman Golesorkhi,[a] Laure Guénée,[b] Homayoun Nozary,[a] Alexandre Fürstenberg,[a] Yan Suffren,[c],[e] Svetlana V. Eliseeva,[d] Stéphane Petoud,*[d] Andreas Hauser*[c] and Claude Piguet*[a]

[a] *Mr. B, Golesorkhi, Dr. H. Nozary, Dr A. Fürstenberg, Prof. Dr C. Piguet Department of Inorganic and Analytical Chemistry University of Geneva, 30 quai E. Ansermet, CH-1211 Geneva 4, (Switzerland). E-mail: Claude.Piguet@unige.ch*

[b] *Dr L. Guénée Laboratory of Crystallography, University of Geneva, 24 quai E. Ansermet, CH-1211 Geneva 4 (Switzerland).*

[c] *Dr. Y. Suffren, Prof. Dr A. Hauser, Department of Physical Chemistry University of Geneva, 30 quai E. Ansermet, CH-1211 Geneva 4 (Switzerland). E-mail: Andreas.Hauser@unige.ch*

[d] *Dr S. V. Eliseeva, Prof. Dr S. Petoud, Centre de Biophysique Moléculaire, CNRS UPR 4301, Rue Charles Sadron, F-45071 Orléans Cedex 2 (France). E-mail : Stephane.Petoud@inserm.fr*

[e] *Current address: Université Rennes, INSA Rennes, CNRS, ISCR "Institut des Sciences Chimiques de Rennes", F-35708 Rennes (France).*

Supporting information and the ORCID identification number(s) for the author(s) of this article can be found under https://doi.org/10.1002/chemxxxxx

Abstract

Intrigued by the unexpected room-temperature dual visible-NIR luminescence observed for fast-relaxing erbium complexes embedded in triple-stranded helicates, this contribution explores a series of six tridentate *N*-donor receptors **L4-L9** with variable aromaticities and alkyl substituents for extricating the stereo-electronic requirements responsible for such scarce optical signatures. Detailed solid state (X-ray diffraction, differential scanning calorimetry, optical spectroscopy) and solution (speciations and thermodynamic stabilities, spectrophotometry, NMR and optical spectroscopy) studies of mononuclear unsaturated $[Er(\mathbf{L}\boldsymbol{k})_2]^{3+}$ and saturated triple-helical $[Er(\mathbf{L}\boldsymbol{k})_3]^{3+}$ model complexes reveal that the stereo-electronic changes induced by the organic ligands affect inter- and intra-molecular interactions to such an extent that (i) melting temperatures in solids, (ii) the affinity for trivalent erbium in solution, and (iii) optical properties in luminescent complexes can be rationally varied and controlled. With this toolkit in hand, mononuclear erbium complexes with low stabilities displaying only near-infrared (NIR) emission can be transformed into molecular-based dual Er-centered visible/NIR emitters operating at room temperature in solids and in solutions.

Introduction

Trivalent neodymium ($4f^3$), holmium ($4f^{10}$), but especially erbium ($4f^{11}$) are famous for possessing a series of regularly spaced $^{2S+1}L_J$ excited spectroscopic levels which cover the entire near-infrared (NIR), visible (VIS) and ultra-violet (UV) domains (Scheme 1).[1] The radiative relaxation processes taking place between the different levels, quantified by their radiative rate constants k_r and lifetimes $\tau_r = 1/k_r$ obey Einstein's probability $A_{J',J}$ (in s^{-1}) of spontaneous $J' \rightarrow J$ emission (Equation (1)), where h is Planck's constant, ν is the energy gap (in frequency unit) between the two incriminated J and J' states, c is the speed of light, g_J and $g_{J'}$ are the degeneracies of states J and J', respectively, and $B_{J,J'}$ is Einstein's coefficient giving the probability per unit time and per unit spectral energy density of the radiation field that an electron in state J absorbs a photon and jumps to state J'.[2]

$$k_r = \frac{1}{\tau_r} = A_{J',J} = \frac{8\pi h\nu^3}{c^3}\frac{g_J}{g_{J'}}B_{J,J'} \quad (1)$$

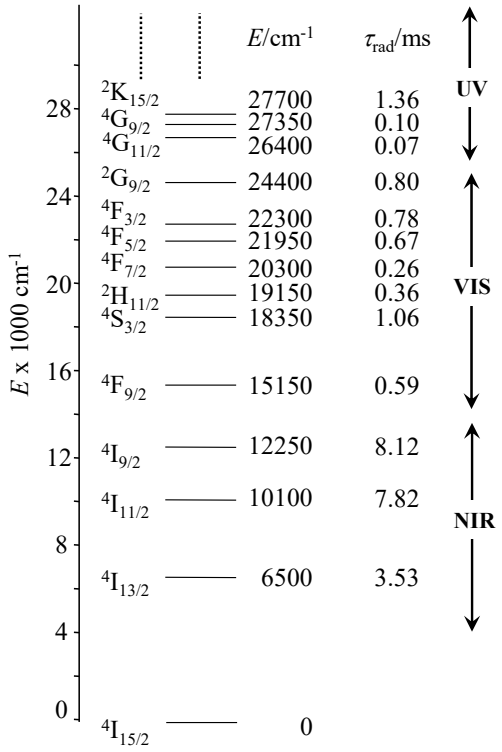

Scheme 1. Details of the near-infrared, visible, and near-ultra-violet parts of the energy-level diagram for Er^{3+} ions doped into yttrium orthoaluminate $YAlO_3$ including calculated radiative lifetimes.[8]

In quantum mechanics, $B_{J,J'}$ is proportional to the square of the transition moment $\langle \phi_J | \hat{H}_p | \phi_{J'} \rangle^2$, where ϕ_J and $\phi_{J'}$ are the wavefunctions of the J and J' states and $\hat{H}_p$ is the electromagnetic-induced perturbation hamiltonian, which involves electric and magnetic dipole components.[3] Within the framework of Judd and Ofelt theory of forced electric dipole intrashell 4f-4f transitions, Eq. (1) transforms into Eq. (2) for estimating the radiative rate constants in a lanthanide complex, where S_{ED} and S_{MD} are the electric-dipole and magnetic-dipole line strengths and n is the refractive index of the medium.[4]

$$k_r = A_{J',J} = \frac{64\pi^4 e^2 \nu^3}{3h(2J+1)} \left[\frac{n(n^2+2)^2}{9} S_{ED} + n^3 S_{MD} \right] \quad (2)$$

Since (i) the maximum energy gap between two adjacent energy levels in trivalent erbium compounds does not exceed $\tilde{\nu}$ = 4000 cm^{-1} (except for the maximum energy gap of 6500 cm^{-1} found between $Er(^4I_{13/2})$ and the ground state $Er(^4I_{15/2})$, Scheme 1) and (ii) the associated dipole line strengths S_{ED}

and S_{MD} are weak for f-f transitions,[4] Eq. (2) predicts small radiative rate constants, *i.e.* long radiative lifetimes spanning the 0.1-10 ms range (Scheme 1, right column).[3],[4] On the other hand, the competitive non-radiative relaxation pathways connecting states *J'* and *J* in trivalent lanthanides imply no significant displacement along any nuclear coordinates: a situation in line with the complete neglect of the Huang-Rhys factors[5] and the simple use of the energy gap law given in Eq. (3). The non-radiative rate constant, k_{nr}, thus decreases exponentially with increasing energy gaps $\Delta E = E_{J'} - E_J$, as measured by the numbers *p* of available high-vibrational modes $\hbar\omega_{max}$ required for filling these intervals (β is a constant of the material).[6]

$$k_{nr} \propto e^{-\beta \Delta E} = e^{-\beta p} \quad (3)$$

In erbium(III)-doped ionic solids or nanoparticles, the effective vibrational energy is low and amounts to $\hbar\omega_{eff} \approx$ 40-100 cm^{-1}, from which $p_{eff} \approx$ 40-100 can be deduced for matching $\Delta E \approx$ 4000 cm^{-1}. In these conditions, Eq. (3) predicts that non-radiative processes are poorly efficient ($k_{nr} \leq k_r$), thus producing long experimental excited lifetimes (close to the radiative lifetimes) and high quantum yields. In erbium(III) coordination complexes, the effective vibrational energy reaches $\hbar\omega_{eff} \approx$ 2000 cm^{-1},[6] and p_{eff} reduces to ≈ 2. Non-radiative relaxation dominates throughout ($k_{nr} >> k_r$) with no hope for detecting luminescence, except for the weak near-infrared Er($^4I_{13/2} \rightarrow {}^4I_{15/2}$) emission at 6500 cm^{-1}, which benefits from $p_{eff} \geq 3$.[7] Since the latter luminescent transition occurs at ca. 1.54 μm, a wavelength which is little attenuated by silica-based optical fibers and by biological tissues, Er^{3+} is attractive for working as activator in lasers, in optical amplifiers exploiting silica,[9] Al_2O_3[10] or $LiNbO_3$ ionic hosts,[11] in plastic waveguides,[12] in organometallic light-emitting diodes[7],[13] and in biological probes and sensors.[14] Major efforts were thus made for maximizing Er($^4I_{13/2} \rightarrow {}^4I_{15/2}$) emission quantum yield in molecular compounds[15] through the minimization of k_{nr} (*i.e.* maximization of the Er($^4I_{13/2}$) excited state lifetime) which accompanies the replacement of high-energy X-H oscillators (X = C, N, O) located close to the activator with heavier X-D and X-F analogues.[16] Such improvements open novel perspectives for inducing linear upconversion into

molecular complexes, a process during which two near-infrared photons are successively absorbed by the erbium activator, prior to be eventually emitted as a single photon of higher energy.[17] This mechanism, referred to as excited state absorption (ESA), was discovered during the late fifties in ionic erbium-doped solids because the millisecond-lived excited states observed in these low-phonon materials (see Scheme 1) are compatible with non-negligible probabilities for these intermediate excited states to catch a second photon leading to doubly excited levels.[18] Linear upconversion was significantly improved few years later by the demonstration that the indirect sensitization may greatly help in feeding the pertinent long-lived erbium-centered excited states (energy transfer upconversion: ETU),[19] and ETU is currently exploited for engineering functional solid materials and nanoparticles.[20]

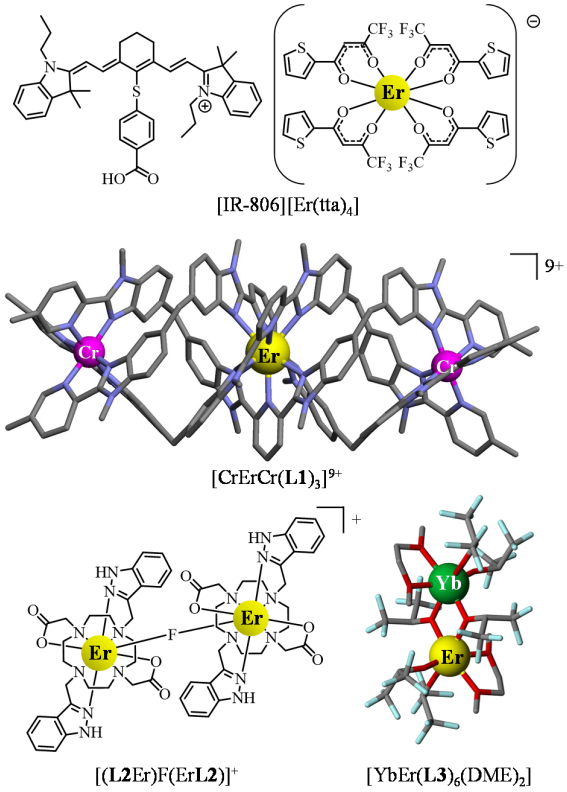

Scheme 2. Erbium-based coordination complexes exhibiting linear upconversion processes via the ETU mechanism. X-ray crystal structures are shown for [CrErCr(**L1**)$_3$](CF$_3$SO$_3$)$_9$ [23] and [YbEr(**L3**)$_6$(DME)$_2$] [25] (color code: C = grey, N = dark blue, O = red, F= light blue). Chemical structures deduced from spectroscopic data recorded in solution are depicted for [IR-806][Er(tta)$_4$] [22] and [(**L2**Er)F(**L2**Er)]$^+$.[24]

To the best of our knowledge, the unambiguous implementation of ESA in molecular complexes under reasonable incident pump intensities (i.e. below 1 kW/cm^2) is currently unknown,[21] and the few successful molecular erbium-centered upconverters reported so far exploit the ETU mechanism as found in [IR-806][Er(tta)$_4$] (use of a polyaromatic sensitizer),[22] [CrErCr(**L1**)$_3$]$^{9+}$(use of a d-block sensitizer),[23] [(**L2**Er)F(Er**L2**)]$^+$ [24] and [YbEr(**L3**)$_6$(DME)$_2$] (use of f-block sensitizers, Scheme 2).[25] Beyond some classical optimization of the sensitization in the latter complexes maximizing NIR absorption cross sections,[22] the ultimate induction of visible Er-centered emission, for instance the green Er(^{4}S$_{3/2}\rightarrow{}^4$I$_{15/2}$) signal, while at least one long-lived intermediate excited state relay of lower energy is available, for instance Er(^{4}I$_{13/2}$), represents a major impediment for the implementation of successful linear piling up of photons in these molecular systems. Looking at erbium chemistry, the latter requirement for multiple (at least dual) emission is commonly fulfilled in solid-state samples and nanoparticles,[17] and uponversion is therefore common in doped solids.[20],[26] The exact mechanism responsible for the feeding of the various emissive levels is still subject of lively debates.[27] On the contrary, molecular erbium complexes, when they are emissive upon ligand-centered UV excitations,[6] usually deliver a single weak near-infrared ^{4}I$_{13/2}\rightarrow{}^4$I$_{15/2}$ emission band, which is diagnostic for the existence of a single long-lived intermediate excited state.[7],[14],[15] In this context, the dual visible Er(^{4}S$_{3/2}\rightarrow{}^4$I$_{15/2}$) (545 nm, $\tau\left({}^4\mathrm{S}_{3/2}\right)$ = 40(2) ns) and near-infrared Er(^{4}I$_{13/2}\rightarrow{}^4$I$_{15/2}$) (1525 nm, $\tau\left({}^4\mathrm{I}_{13/2}\right)$ = 3.6(3) μs) emission bands arising from the pseudo-tricapped trigonal prismatic ErN$_9$ site in [CrErCr(**L1**)$_3$]$^{9+}$ (Scheme 2) appears to be particularly intriguing because no special care was taken for replacing H atoms with D or F atoms in the ligand strand.[23] We report here on our efforts for identifying, by structural 'dissection' in ligands **L4**-**L9** (Schemes 3-4), the chemical design required for the successful induction of room-temperature dual visible/near infrared emissions in stable ErN$_9$ coordination sites: a prerequisite for the design of erbium-containing molecular light-upconverters.

Results and Discussions

Tridentate receptors L4-L9: synthesis and substituent effects.

A careful look at the crystal structure of [CrErCr(**L1**)$_3$]$^{9+}$ cation (Scheme 2), suggests that the target central luminescent ErN$_9$ site could be reproduced in a mononuclear model *via* the helical wrapping of three 2,6-bis(benzimidazol-2-yl)pyridine ligands around a trivalent lanthanide cation as found in [Eu(**L4**)$_3$](ClO$_4$)$_3$,[28] [Eu(**L4'**)$_3$](ClO$_4$)$_3$ (**L4'** is identical to **L4**, except for the replacement of *N*-methyl groups with *N*-neopentyl analogues)[29] and [Eu(**L5'**)$_3$](ClO$_4$)$_3$ (**L5'** is identical to **L5** except for the replacement of *N*-methyl groups with *N*-ethyl analogues, see Scheme 3).[30] However, repulsive intramolecular inter-strand interactions produced by the tight wrapping of three ligands around the metallic cation in [Eu(**L4**)$_3$]$^{3+}$ is thought to be responsible for the unsuccessful isolation of related complexes using cations smaller than Eu(III) along the lanthanide series.[31]

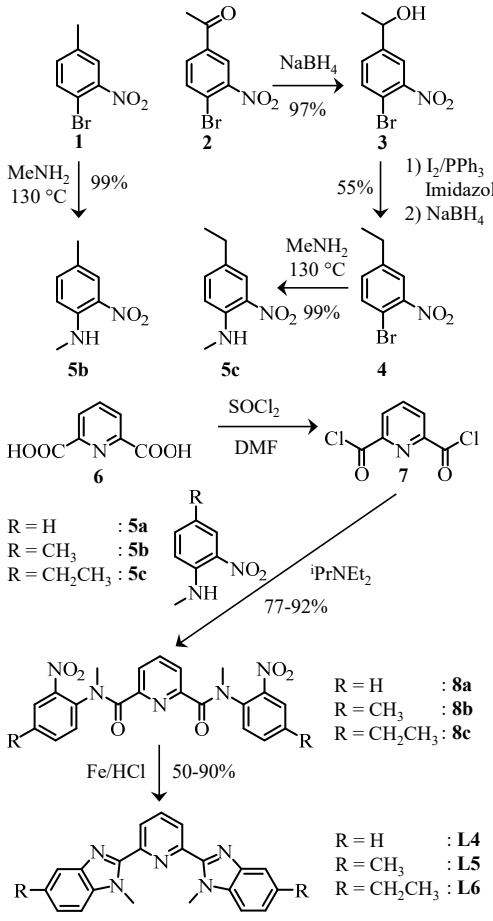

Scheme 3. Synthesis of 2,6-bis(5,5'-disubstituted-benzimidazol-2-yl)pyridine ligands **L4-L6**.

Since the ionic radius of the target Er^{3+} cation is significantly smaller than that of Eu^{3+}, we exploited compact *N*-methyl substituents for minimizing spatial expansion in ligands **L4-L6,** together with the connection of terminal alkyl substitution of increasing size R = H (**L4**) < R= CH_3 (**L5**) < R = CH_2CH_3 (**L6**) for preventing any infiltration of inner-sphere solvent molecules and/or counter-anions into the core of the target $[Ln(\mathbf{L}\boldsymbol{k})_3]^{3+}$ triple helices. The syntheses of the bis-benzimidazolpyridine series (bisbzimpy: **L4-L6**) rely on the well-established two-step reductive Philips-modified reaction of activated dipicolinic acid **7** with substituted ortho-nitroaminophenyl derivatives **5a-c**.[32] The synthesis of **L4**, which used commercially available **5a**, was previously reported.[28],[30] Analogous 5-methyl derivatives **5b** and the 5-ethyl derivative **5c** can be easily obtained by aryl nucleophilic substitution of adapted ortho-bromo-nitrophenyls **1** and **4**,[33] thus leading to ligands **L5** and **L6** (Scheme 3).

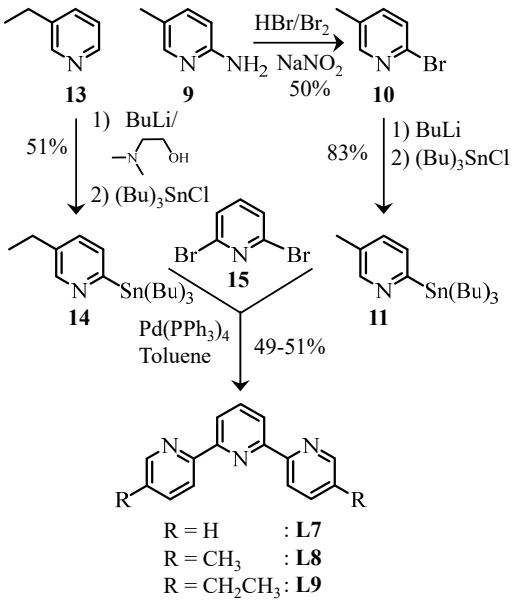

Scheme 4. Synthesis of 5,5''-disubstituted 2,2':6',2"-terpyridine ligands **L7**-**L9**.

Interestingly, the closely related, but less extended 2,2':6',2"-terpyridine ligand **L7** is known to produce stable triple-helical $[Ln(\mathbf{L7})_3]^{3+}$ along the complete lanthanide series, this without size-discriminating effects.[34] It would be highly desirable to prepare the analogous terpyridine series (terpy: **L7**-**L9**) for comparison purpose. Initial attempts to prepare the methyl (**L8**) and ethyl (**L9**) derivatives using catalyzed alkyl/aryl cross-coupling reactions with 5,5"-dichloroterpyridine[35] gave

only low yields (< 20%) in our hands. A more successful approach used double Stille-type cross-coupling reactions between 2,6-dibromopyridine **15**[36] and stannylated 5-methylpyridine **11**[37] and 5-ethylpyridine **14** (Scheme 4).[38]

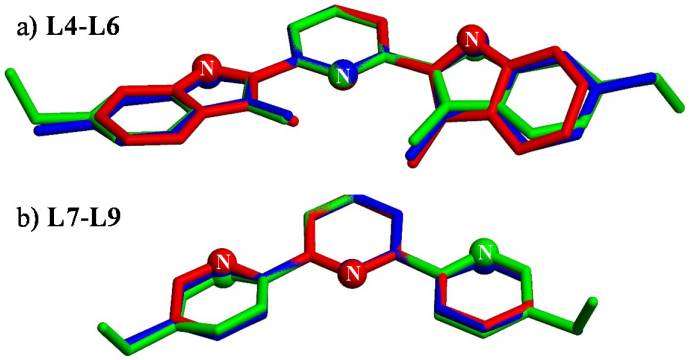

Figure 1. Superimposition of molecular structures of a) **L4** (red), **L5** (blue) and **L6** (green) and b) **L7** (red), **L8** (blue) and **L9** (green) as observed in their crystal structures. Hydrogen atoms are omitted for clarity and N-donor atoms are highlighted.

As previously observed in the crystal structures of **L4**[39] and **L7**,[40] the three connected heterocyclic units in **L5-L6** and **L8-L9** adopt pseudo-twofold *transoid-transoid* arrangements of the nitrogen donor atoms (Figure 1, Tables S1-S13 and Figure S1 in the Supporting Inofrmation). Variable interplanar angles between the connected aromatic heterocycles ($7.2 \leq \omega \leq 42.8°$) result from specific intermolecular inter-aromatic packing interactions observed in the crystals (Figure S2). A thorough thermodynamic analysis of the ligand melting processes (Figures S3-S8 and Appendix 1) within the framework of enthalpy/entropy compensation,[41] combined with cohesive free energy densities,[42] leads to the conclusion that the H→CH_3→CH_2CH_3 sequence implemented in **L4→L5→L6** and **L7→L8→L9** series produces two successive, but opposite changes in intermolecular cohesion in the solid state. The replacement of small hydrogen atoms with methyl groups improves the cohesion due the increase in molecular polarizability, while further extension provided by the introduction of additional methylene rotors to give non-linear ethyl substituents severely disrupts the inter-aromatic stacking. These three-dimensional substituent-induced packing effects, identified for the free ligand **L4-L9** in the solid state**,** have their molecular (*i.e.* zero-dimensional) counterpart in the target triple

helices $[Ln(\mathbf{Lk})_3]^{3+}$ where alkyl-modulated intramolecular inter-strand interactions are known to control metal protection and crystal-field parameters.[28]-[31]

Erbium complexes with receptors L4-L9: speciation, stabilities and solution structures. Electrospray-ionization mass spectroscopy (ESI-MS) titrations of ligands **L4** (bisbzimpy) and **L7** (terpy) with $Er(CF_3SO_3)_3$ in acetonitrile show the stepwise formation of $[Er(\mathbf{Lk})_n]^{3+}$ (n = 3-1) with some gas-phase adducts $[Er(\mathbf{Lk})_n(CF_3SO_3)_i]^{(3-i)+}$ in agreement with Equilibria (4)-(6) (Figures S9-S10, Supporting Information).

$$Er^{3+}_{solvated} + \mathbf{Lk} \rightleftharpoons \left[Er(\mathbf{Lk})\right]^{3+}_{solvated} \qquad \beta^{Er,\mathbf{Lk}}_{1,1} \qquad (4)$$

$$Er^{3+}_{solvated} + 2\,\mathbf{Lk} \rightleftharpoons \left[Er(\mathbf{Lk})_2\right]^{3+}_{solvated} \qquad \beta^{Er,\mathbf{Lk}}_{1,2} \qquad (5)$$

$$Er^{3+}_{solvated} + 3\,\mathbf{Lk} \rightleftharpoons \left[Er(\mathbf{Lk})_3\right]^{3+}_{solvated} \qquad \beta^{Er,\mathbf{Lk}}_{1,3} \qquad (6)$$

Beyond the ESI-MS signals observed for the protonated ligands $[\mathbf{Lk}+n\mathrm{H}]^{n+}$, the intensity of which are biased by their efficient gas-phase transfer coefficients,[43] only few faint ESI-MS signals can be detected. They correspond to traces of hydrolyzed dimeric complexes $[(\mathbf{Lk})_2Er(OH)_2Er(\mathbf{Lk})_2]^{4+}$ which will therefore not be considered further in the thermodynamic modeling of the speciation. ^{1}H NMR titrations of the methyl-substituted ligands **L5** and **L8**, which were selected for the simple first-order analysis of their spin systems upon complexation with diamagnetic $Y(CF_3SO_3)_3$ (the size of Y^{3+} is close to that of Er^{3+}) confirm Equilibria (4)-(6) and the formation of only three complexes $[Y(\mathbf{Lk})_n]^{3+}$ (n = 3-1) in acetonitrile at millimolar concentrations (Figures 2 and S11-S13). The strong downfield shifts observed for H3 ($\Delta\delta$ = 0.8-0.9 ppm), and to a lesser extend for the methyl groups H6 ($\Delta\delta$ = 0.5 ppm), between the free ligand and the 1:3 complexes $[Y(\mathbf{Lk})_3]^{3+}$ are diagnostic for the formation of a triple helix (magenta dashed traces in Figures 2 and S11-S13), which puts these protons in the shielding region of the terminal aromatic groups of the next ligand strands.[28],[30] As expected, this effect is stepwise relaxed with the successive loss of ligand strands when $[Y(\mathbf{Lk})_3]^{3+}$ transforms into $[Y(\mathbf{Lk})_2]^{3+}$ and $[Y(\mathbf{Lk})]^{3+}$ (orange dashed traces in Figures 2 and S11-S13).

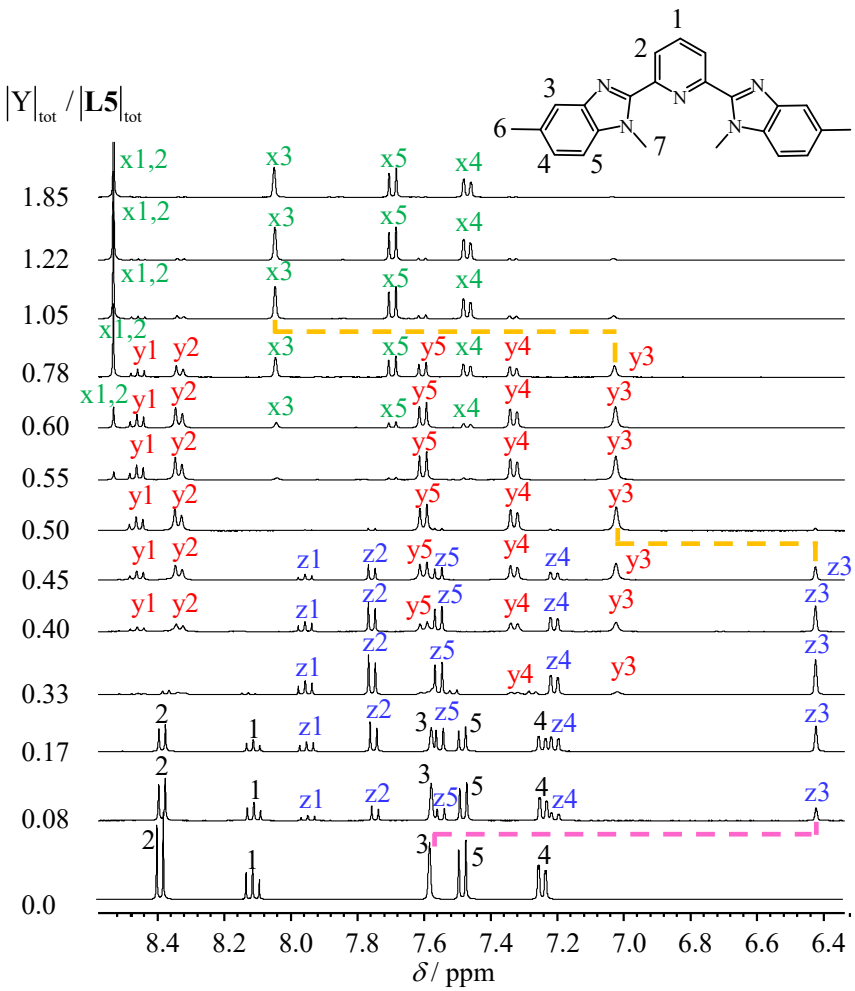

Figure 2. Aromatic parts of the ^{1}H NMR spectra with numbering scheme recorded upon titration of **L5** with $Y(CF_3SO_3)_3$ in CD_3CN at 298 K with numbering scheme. ($5\times10^{-3} \leq |\mathbf{L5}|_{tot} \leq 9\times10^{-3}$ M and $6\times10^{-4} \leq |Y|_{tot} \leq 8\times10^{-3}$ M). The letters x, y and z denote signals arising from the 1:1 (green), 1:2 (red) and 1:3 (blue) species, respectively.

The associated speciation (dots in Figures 3a and S14a) can be obtained by simple integration of the ^{1}H NMR signals of the same proton in ligands ($I_{\mathbf{L}k}$) and complexes ($I_{Y(\mathbf{L}k)n}$, Eq. (7) middle). Only partial binding isotherms could be obtained (occupancy factors $\theta_Y > 60\%$; diamonds in Figures 3b and S14b) because the NMR technique is not sensitive enough to fix total concentrations of metal and ligands low enough to limit binding-site saturation. Attempts to fit the available occupancy factors θ_Y with Eq. (7) gives only mere estimations of the stability constants $\beta_{1,n}^{\mathrm{Er},\mathbf{L}k}$ (gathered in the captions of Figures 3 and S14), which are then used for the calculation of the theoretical speciation curves and binding isotherms (full traces in Figures 3 and S14).

$$\theta_{Y} = \frac{1}{3}\frac{|\mathbf{Lk}|_{bound}}{|Y|_{tot}} = \frac{1}{3}\frac{(I_{YLk} + I_{Y(Lk)_2} + I_{Y(Lk)_3})|\mathbf{Lk}|_{tot}}{(I_{Lk} + I_{YLk} + I_{Y(Lk)_2} + I_{Y(Lk)_3})|Y|_{tot}} = \frac{1}{3}\frac{\sum_{n=1}^{3} n\beta_{1,n}^{Y,Lk}\left(|\mathbf{Lk}|\right)^{n}}{1+\sum_{n=1}^{3}\beta_{1,n}^{Y,Lk}\left(|\mathbf{Lk}|\right)^{n}} = \frac{1}{3}\frac{|\mathbf{Lk}|_{tot} - |\mathbf{Lk}|}{|Y|_{tot}} \quad (7)$$

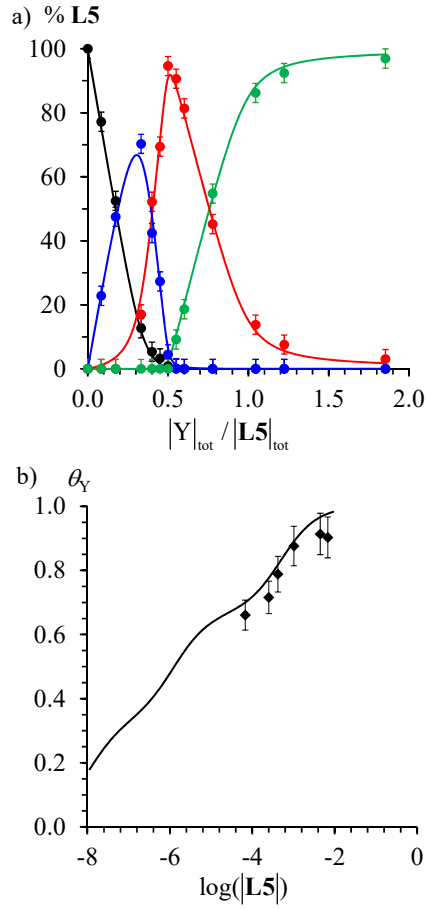

Figure 3. a) Macroscopic ligand speciations (dots) obtained by integration of ^{1}H NMR signals during the titration of **L5** (1.6×10^{-2} mol·dm^{-3}) with $Y(CF_3SO_3)_3$ in CD_3CN at 298 K (black = **L5**, blue = $[Y(\mathbf{L5})_3]^{3+}$, red = $[Y(\mathbf{L5})_2]^{3+}$ and green = $[Y(\mathbf{L5})]^{3+}$) and b) associated binding isotherm (Eq. (7); diamonds). The full traces correspond to the re-constructed a) distribution and b) binding isotherm computed using Equilibria (4)-(6) with $\beta_{1,1}^{Y,L5} = 8.0$, $\beta_{1,2}^{Y,L5} = 13.9$ and $\beta_{1,3}^{Y,L5} = 17.2$.

As expected for ligand-metal association reactions (Eqs 4-6) monitored in weakly polar organic media, the disruption of the chemical potential of the solvent induces a dependence of the quotient of the reaction on the advance of the complexation process.[44] This prevents a simple determination of the true thermodynamic constants $\beta_{1,n}^{Er,Lk}$, which are then obtained as rough average values from the ^{1}H NMR data.[45] The associated binding isotherms depicted in Figures 3b and S14b therefore only

roughly fit the theoretical curves predicted with Eq. 7. Pertinent values for $\beta_{1,n}^{\mathrm{Er},\mathbf{Lk}}$ are restored when titrations are recorded at much lower concentrations by spectrophotometry (vide infra). Related ^{1}H NMR titrations with ethyl-substituted ligands **L6** and **L9** obviously give very similar results (Figures S15-S16), but the hydrogen atoms of the methylene probes are systematically enantiotopic (pure quartets). This results points to the presence of time-averaged symmetry planes on the NMR time scale for all complexes including, to our surprise, the D_3-symmetrical triple helical complexes $[Y(\mathbf{Lk})_3]^{3+}$. Making the assumption that a dynamic symmetry plane results from fast exchange between the two D_3-helical enantiomers on the NMR time scale, as previously reported for lanthanide tris-dipicolinates,[46] low-temperature NMR data were collected, but they did not improve the situation. However, it is worth reminding here that the experimentally accessible dynamic range of an exchange process as measured by two diastereotopic protons depends on the difference of the specific chemical shifts in absence of exchange $\Delta\nu$, which fixes the coalescence temperature T_c for a given free energy barrier $\Delta G^{\neq}$ (Eq. (8), k_B and h are respectively the *Boltzmann* and the *Planck* constants).[47] For diamagnetic yttrium complexes $[Y(\mathbf{Lk})_3]^{3+}$, the two hydrogen atoms of the methylene probe likely display very similar chemical environments (i.e $\Delta\nu$ is small) and T_c lies thus much below 233 K, the minimum accessible temperature in acetonitrile.

$$\Delta G^{\neq} = RT\ln\left(\frac{\sqrt{2}\cdot k_B\cdot T_c}{h\cdot\pi\cdot\Delta\nu}\right) \qquad (8)$$

Replacing Y(III) with paramagnetic Er(III) boosts the difference in chemical shifts between the methylene hydrogen atoms H6 and H6'. Two signals, separated by $\Delta\nu$ = 220 Hz, are now recorded for $[Er(\mathbf{L9})_3]^{3+}$ at room temperature, in agreement with the existence of a 'blocked' triple-helical arrangement in solution (Figure S17, Supporting Information). High-temperature ^{1}H NMR data combined with linear extrapolation give an estimation of T_c = 433(34) K, from which $\Delta G^{\neq}$ = 59(4) kJ/mol can be computed with Eq. (8) for the intramolecular helical interconversion. The latter values compares well with $\Delta G^{\neq}$(Tm) = 64(1) kJ/mole (T_c = 290 K) and $\Delta G^{\neq}$(Yb) = 60(1) kJ/mole (T_c = 303

K) previously reported for related intramolecular helical exchange processes occurring in D_3-symmetrical $[Ln(2,6\text{-dipicolinate})_3]^{3-}$ in D_2O.[46]

Having established that the speciation in solution obeys Equilibria (4)-(6), pertinent thermodynamic stability constants were obtained by spectrophotometric titrations of **L*k*** with $[ErX_3]$ (X = $CF_3SO_3^-$, ClO_4^- and $[Al(OC(CF_3)_3)_4]^-$) collected at low concentration in acetonitrile (Figures 4a,b and Figures S18-S22). Evolving factor analysis[48] confirms the existence of four absorbing species (Figure 4c), while non-linear least-square fit[49] to Equilibria (4)-(6) provide stability constants (Table 1) together with acceptable reconstructed absorption spectra (Figure 4d).

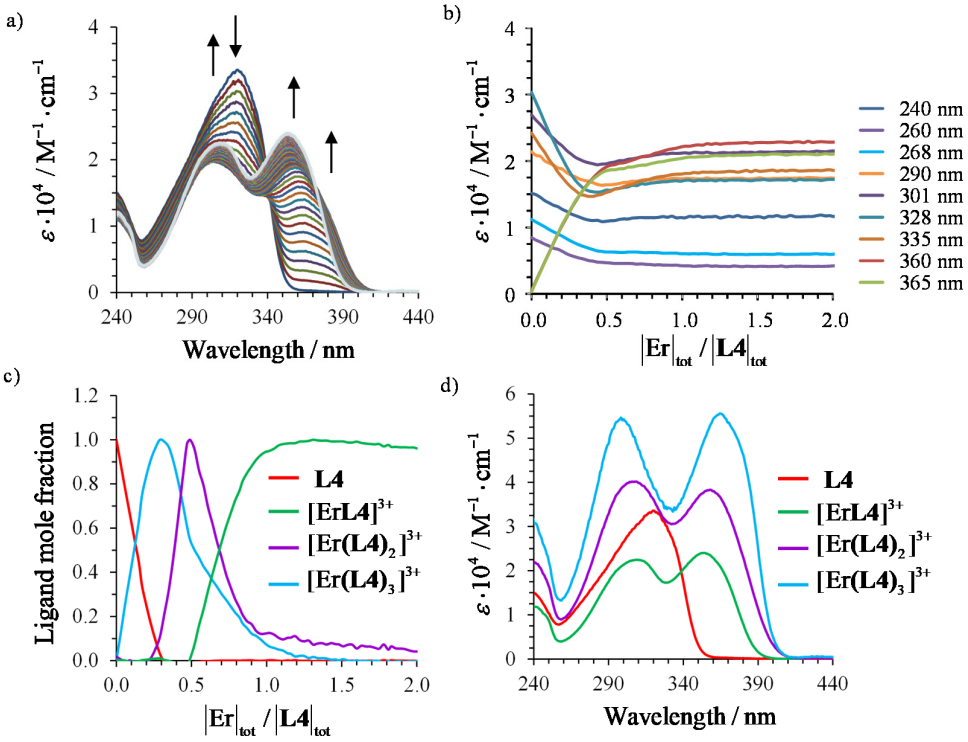

Figure 4. a) Variation of experimental absorption spectra and b) corresponding variation of molar extinction at different wavelengths observed for the spectrophotometric titration of **L4** with $Er(CF_3SO_3)_3$ (total ligand concentration: 3.0×10^{-4} M in acetonitrile, 298 K). c) Evolving factor analysis[48] using four absorbing eigenvectors and d) reconstructed individual electronic absorption spectra.

Since poorly coordinating triflate ($CF_3SO_3^-$) or perchlorate (ClO_4^-) anions are known to display similar affinities for Er^{3+},[50] the stability constants $\beta_{1,n}^{Er,Lk}$ obtained in the presence of these counter-anions for complexing **L4** and **L7** are logically similar (Table 1, entries 1-8). On the contrary, the use

of less-coordinating perfluoroalkoxyaluminate anions $[Al(OC(CF_3)_3)_4]^-$ [51] further increases the affinity of Er^{3+} for ligands **L4**-**L9** by one order of magnitude (Table 1, entries 9-14).

Table 1. Thermodynamic formation constants $\log(\beta_{1,n}^{Er,Lk})$ (Equations (4)-(6)) and associated microscopic parameters $\Delta G_{affinity}^{Er,Lk} = -RT\ln(f^{Er,Lk})$ and $\Delta E^{Lk,Lk} = -RT\ln(u^{Lk,Lk})$ (Equations (9)-(11) obtained for the spectrophotometric titrations of **L4**-**L9** with ErX_3 (X= $CF_3SO_3^-$, ClO_4^-, $[Al(OC(CF_3)_3)_4]^-$) in acetonitrile at 298 K.

L*k*	Anion	$\log(\beta_{1,1}^{Er,Lk})$	$\log(\beta_{1,2}^{Er,Lk})$	$\log(\beta_{1,3}^{Er,Lk})$	$\Delta G_{affinity}^{Er,Lk}$ kJ·mol^{-1}	$\Delta E^{Lk,Lk}$ kJ·mol^{-1}
L4	ClO_4^-	9.6(1)	17.4(4)	22.7(4)	-51(1)	10(1)
L7	ClO_4^-	9.8(1)	17.1(1)	22.5(1)	-50.7(3)	11(1)
L4	$CF_3SO_3^-$	9.2(1)	16.5(3)	20.9(3)	-49(1)	11(1)
L5	$CF_3SO_3^-$	10.9(4)	20.2(8)	24.8(8)	-60(3)	15(4)
L6	$CF_3SO_3^-$	11.6(5)	22(1)	26(1)	-66(5)	19(6)
L7	$CF_3SO_3^-$	10.5(2)	18.5(4)	23.0(4)	-56(1)	15(1)
L8	$CF_3SO_3^-$	9.9(1)	17.8(2)	22.7(2)	-53(1)	12(1)
L9	$CF_3SO_3^-$	9.2(1)	16.7(2)	21.8(2)	-49(1)	10(1)
L4	$[Al(OC(CF_3)_3)_4]^-$	10.4(3)	19.3(5)	25.7(7)	-56(1)	9(1)
L5	$[Al(OC(CF_3)_3)_4]^-$	12.0(2)	20.9(4)	27.1(4)	-63.9(1)	14.7(1)
L6	$[Al(OC(CF_3)_3)_4]^-$	12.9(3)	22.8(7)	29.5(8)	-69.6(5)	15.7(6)
L7	$[Al(OC(CF_3)_3)_4]^-$	11.2(2)	19.9(3)	26.8(5)	-59.1(4)	10.5(4)
L8	$[Al(OC(CF_3)_3)_4]^-$	10.4(1)	18.5(2)	24.8(3)	-54.7(2)	9.9(2)
L9	$[Al(OC(CF_3)_3)_4]^-$	10.1(1)	18.6(3)	24.7(3)	-54(1)	9(1)

A global thermodynamic analysis exploits the site-binding model, which considers the successive complexation of tridentate ligands to Er^{3+} within the frame of next-neighbor *Ising*-like interacting chains.[52] According to this simple approach, the purely entropic contributions produced by the

change in rotational entropies (*i.e.* the statistical factors) are safely estimated with the help of symmetry numbers to give the numerical values given in Equations (9)-(11) (see Figure S23 for calculations).[53] The free energy change accompanying the chemical reaction is then partitioned between the simple intermolecular affinity (including solvation effects) accompanying the complexation of Er^{3+} to a single ligand **L*k*** ($\Delta G_{\text{affinity}}^{\text{Er,L}k} = -RT\ln(f^{\text{Er,L}k})$), and the modulation of the latter affinity due to successive ligand binding in $[Er(\mathbf{L}k)_n]^{3+}$ ($n \geq 2$); a thermodynamic correction $\Delta E^{\mathbf{L}k,\mathbf{L}k} = -RT\ln(u^{\mathbf{L}k,\mathbf{L}k})$ often referred to as allosteric cooperativity (eqs 9-11).[54]

$$\beta_{1,1}^{\text{Er,L}k} = 6f^{\text{Er,L}k} \quad (9)$$

$$\beta_{1,2}^{\text{Er,L}k} = 12\left(f^{\text{Er,L}k}\right)^2 u^{\mathbf{L}k,\mathbf{L}k} \quad (10)$$

$$\beta_{1,3}^{\text{Er,L}k} = 16\left(f^{\text{Er,L}k}\right)^3 \left(u^{\mathbf{L}k,\mathbf{L}k}\right)^3 \quad (11)$$

Multi-linear least-square fits of the experimental successive stability constants $\log(\beta_{1,n}^{\text{Er,L}k})$ to the logarithmic forms of Equations (9)-(11) provide $\Delta G_{\text{affinity}}^{\text{Er,L}k} = -RT\ln(f^{\text{Er,L}k})$ and $\Delta E^{\mathbf{L}k,\mathbf{L}k} = -RT\ln(u^{\mathbf{L}k,\mathbf{L}k})$ gathered in Table 1 (columns 6-7) and illustrated in Figure 5. As expected, the intrinsic metal-ligand affinities are favored when triflate anions are replaced with the less competitive counter-anion $[Al(OC(CF_3)_3)_4]^-$, but the successive connections of alkyl groups of larger sizes at the termini of the ligands induce surprising opposite trends when plotting $\Delta G_{\text{affinity}}^{\text{Er,L}k}$ along the bisbzimpy series (**L4**-**L6**) and terpy (**L7**-**L9**) series (Figure 5a). The latter behavior is paralleled by the anti-cooperative interligand interactions $\Delta E^{\mathbf{L}k,\mathbf{L}k}$ (Figure 5b). The regular dependence of both intrinsic affinities and interligand interactions on the molecular volumes[55] within each series suggests the prevalence of solvation effects in controlling the thermodynamic binding properties as previously established for helicate self-assemblies[56] and for the metal loading of linear polymers.[57] Pertinent Born-Haber cycles developed in Appendix 2 demonstrate that, whilst the thermodynamic stabilities of the $[Er(\mathbf{L}k)_n]^{3+}$ (n = 1-3) complexes in acetonitrile are globally comparable for all six ligands, the minor variations along the series observed in Figure 5 can be rationalized by a fine balance between

inductive effect and size-dependent solvation energies. Specific inter-strand interactions can be highlighted in $[Er(\mathbf{L5})_3]^{3+}$ and $[Er(\mathbf{L6})_3]^{3+}$ when three bulky extended aromatic ligands are wrapped around small Er^{3+}.

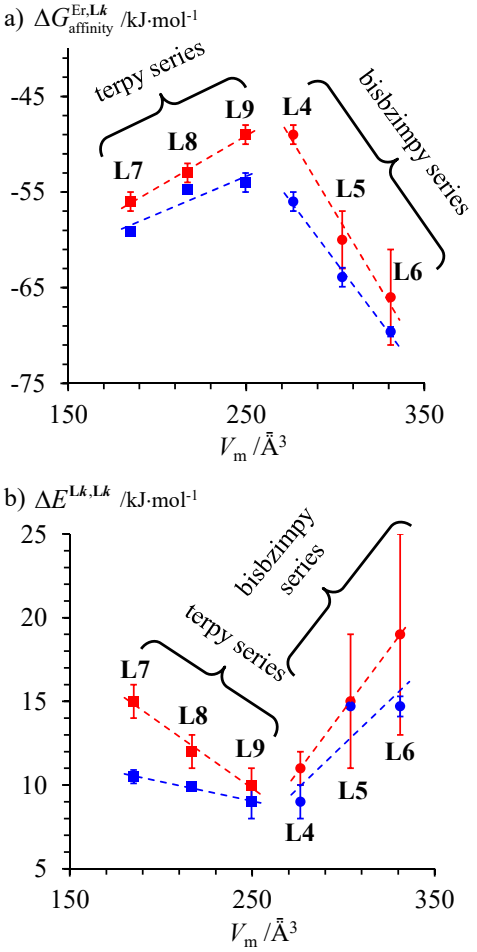

Figure 5. a) Intermolecular microscopic affinities $\Delta G^{Er,Lk}_{affinity} = -RT\ln(f^{Er,Lk})$ for inner sphere connection of $Er(CF_3SO_3)_3$ (red) and $Er([Al(OC(CF_3)_3)_4])_3$ (blue) to the tridentate binding sites in ligands **L4-L9** (CH_3CN, 298 K). b) Interligand interactions $\Delta E^{Lk,Lk} = -RT\ln(u^{Lk,Lk})$ operating upon successive binding of **L4-L9** to a single metallic center in $Er(CF_3SO_3)_3$ (red) and $Er([Al(OC(CF_3)_3)_4])_3$ (blue). V_m is the molecular volume of the ligand taken as its Connolly volume.[55] The dashed trendlines are only guides for the eyes.

Erbium complexes with receptors L4-L9: isolation and solid-state structures.

According to the stability constants collected in Table 1, we used close to molar concentrations of ligands and ErX_3 salts at 3:1 stoichiometric ratio for producing ≥ 98% of $[Er(\mathbf{L}k)_3]^{3+}$ in acetonitrile

(Figures S24-S25), prior to exposing resulting mixtures either to slow evaporation or to the diffusion of poorly polar volatile solvents for inducing crystallization. In the presence of triflate counter-anions (X = $CF_3SO_3^-$), only 1:2 complexes could be crystallized (Figure 6a, Tables S14-S20 and Figures S26-S28). Since the latter stoichiometry accounts for a maximum 2% of the ligand speciation in solution, these complexes are probably much less soluble than the lipophilic 1:3 adducts. Complexes $[Er(\mathbf{L4})_2(CF_3SO_3)_2](CF_3SO_3)$ (**1**) and $[Er(\mathbf{L7})_2(CF_3SO_3)_2](CF_3SO_3)$ (**2**)[21a] display eight-coordinate Er(III) centers, the coordination geometry of which can be assigned to slightly distorted square antiprisms. Trivalent erbium in $[Er(\mathbf{L8})_2(CF_3SO_3)_3]$ (**3**) is nine-coordinated in a pseudo-tricapped trigonal prismatic coordination sphere (Figure S29).

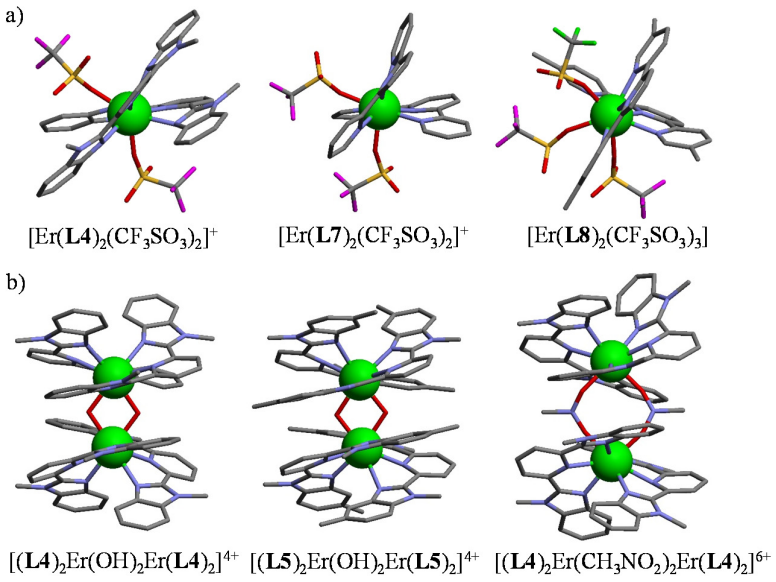

Figure 6. Molecular structures of a) mononuclear 1:2 complexes and b) dinuclear 2:4 complexes found in the crystal structures of $[Er(\mathbf{L4})_2(CF_3SO_3)_2](CF_3SO_3)\cdot 2CH_3CN$ (**1**), $[Er(\mathbf{L7})_2(CF_3SO_3)_2](CF_3SO_3)\cdot 1.5C_2H_5CN$ (**2**),[21a] $[Er(\mathbf{L8})_2(CF_3SO_3)_3]$ (**3**), $[(\mathbf{L4})_2Er(OH)_2Er(\mathbf{L4})_2](ClO_4)_4\cdot 2C_6H_5CN\cdot 4CH_3CN$ (**8**), $[(\mathbf{L5})_2Er(OH)_2Er(\mathbf{L5})_2](ClO_4)_4\cdot C_6H_5CN\cdot 8CH_3CN$ (**9**) and $[(\mathbf{L4})_2Er(CH_3NO_2)_2Er(\mathbf{L4})_2](ClO_4)_6\cdot CH_3NO_2$ (**10**). The counter-anions, solvent molecules and H atoms are omitted for clarity. Color code: C = grey, blue = N, red = O, yellow = S, magenta = F, green = Er.

Replacing triflate with perchlorate counter-anions reduces the solubility of the triple helices $[Er(\mathbf{L}\boldsymbol{k})_3]^{3+}$, which quantitatively crystallized to give $[Er(\mathbf{L6})_3](ClO_4)_3$ (**4**), $[Er(\mathbf{L7})_3](ClO_4)_3$ (**5**), $[Er(\mathbf{L8})_3](ClO_4)_3$ (**6**) and $[Er(\mathbf{L9})_3](ClO_4)_3$ (**7**, Figure 7, Tables S21-S29 and Figures S30-S33). The

nine-coordinate Er(III) sites in these complexes systematically adopt pseudo-tricapped trigonal prismatic geometries (Figure S34). The detailed analysis of Er-N bond distances within the framework of bond valence theory (Table S30)[58] logically confirms that the Er-N interactions in eight-coordinate $[Er(\mathbf{L4})_2(CF_3SO_3)_2]^+$ and $[Er(\mathbf{L7})_2(CF_3SO_3)_2]^+$ complexes are slightly stronger than those found in the corresponding nine-coordinated analogues $[Er(\mathbf{L8})_2(CF_3SO_3)_3]$, $[Er(\mathbf{L}k)_3]^{3+}$ (**L*k* = L6-L9**), $[Eu(\mathbf{L4})_3]^{3+}$ [28],[30] and $[Lu(\mathbf{L7})_3]^{3+}$.[34b] We also note that a significant intramolecular inter-strand packing[59] produced by the tight wrapping of the helical strands in $[Eu(\mathbf{L4})_3]^{3+}$ [28],[30] and $[Er(\mathbf{L6})_3]^{3+}$ (Figure 7 top left and Figure S36) are lacking for the terpy series.

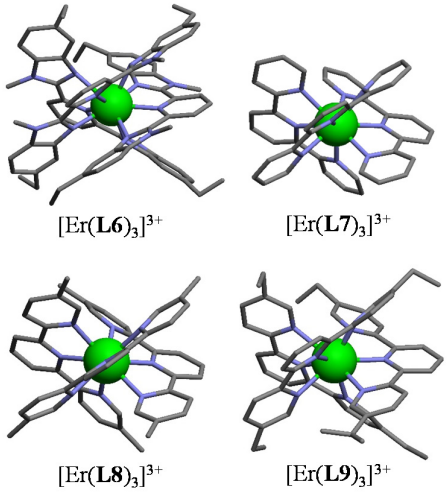

Figure 7. Molecular structures of mononuclear 1:3 complexes found in the crystal structures of $[Er(\mathbf{L6})_3](ClO_4)_3\cdot 1.5CH_3CN$ (**4**), $[Er(\mathbf{L7})_3](ClO_4)_3$ (**5**), $[Er(\mathbf{L8})_3](ClO_4)_3$ (**6**) and $[Er(\mathbf{L9})_3](ClO_4)_3\cdot 1.5CH_3CN$ (**7**). The counter-anions, solvent molecules and H atoms are omitted for clarity. Color code: C = grey, blue = N, green = Er.

In line with previous unsuccessful attempts to isolate Lu-based triple helical complexes with **L4** and **L5** in the solid state,[28],[30] we were unable to isolate $[Er(\mathbf{L}k)_3](ClO_4)_3$ with these two ligands. Slow evaporation of $Er(ClO_4)_3$/**L*k*** (1:3) mixtures (k = 4, 5) over several weeks provided only small quantities of dinuclear complexes $[(\mathbf{L4})_2Er(OH)_2Er(\mathbf{L4})_2](ClO_4)_4$ (**8**), $[(\mathbf{L5})_2Er(OH)_2Er(\mathbf{L5})_2](ClO_4)_4$ (**9**) and $[(\mathbf{L4})_2Er(CH_3NO_2)_2Er(\mathbf{L4})_2](ClO_4)_6$ (**10**), the stoichiometry of which is reminiscent of mononuclear 1:2 complexes (Figure 6b, Tables S31-S37 and Figures S36-S38). According to the fact that no identified thermodynamic effect specifically destabilizes $[Er(\mathbf{L}k)_3]^{3+}$ complexes with **L4** and

L5 (Table 1), we conclude that mass transfers at the solid/solution phase interfaces master solubility during the crystallization processes and the compositions of the resulting solid state samples do not mirror the thermodynamic speciation.

Erbium complexes with receptors L4-L9: dual visible/near-infrared luminescence.

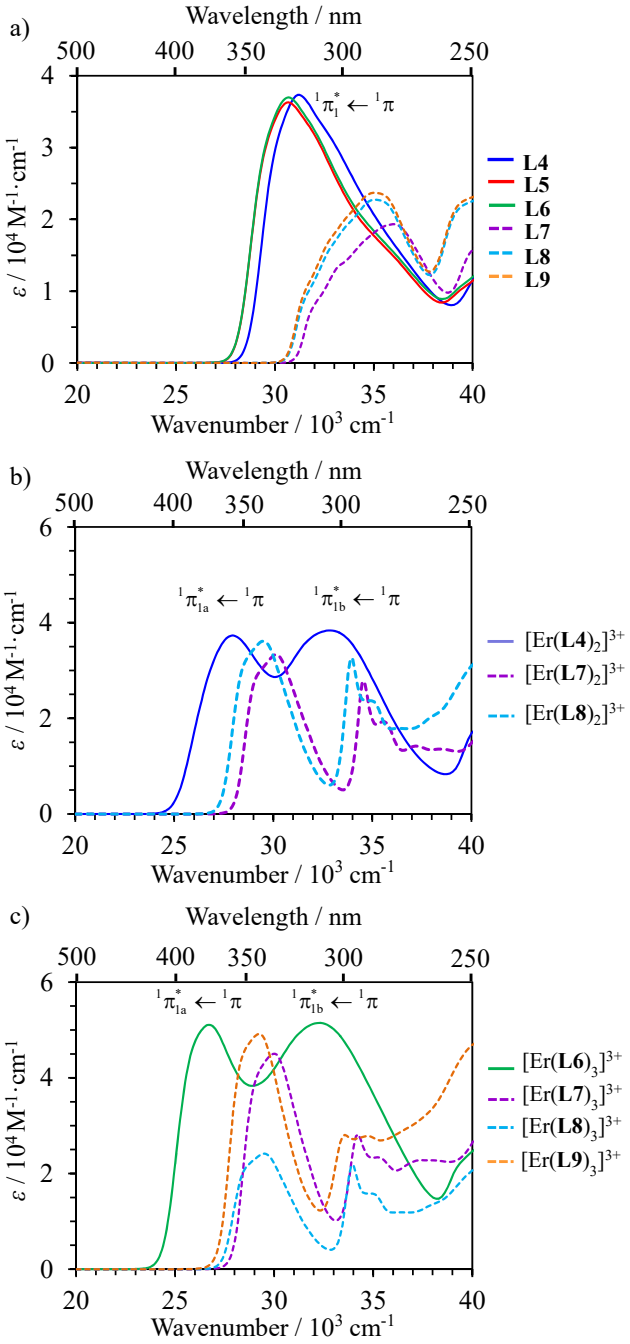

Figure 8. Absorption spectra of a) ligands **L4-L9** (0.3 mM), b) 1:2 complexes **1-3** (3.0 mM) and c) 1:3 complexes **4-7** (3.0 mM) in acetonitrile solution at 298K.

10.1002/chem.201802277

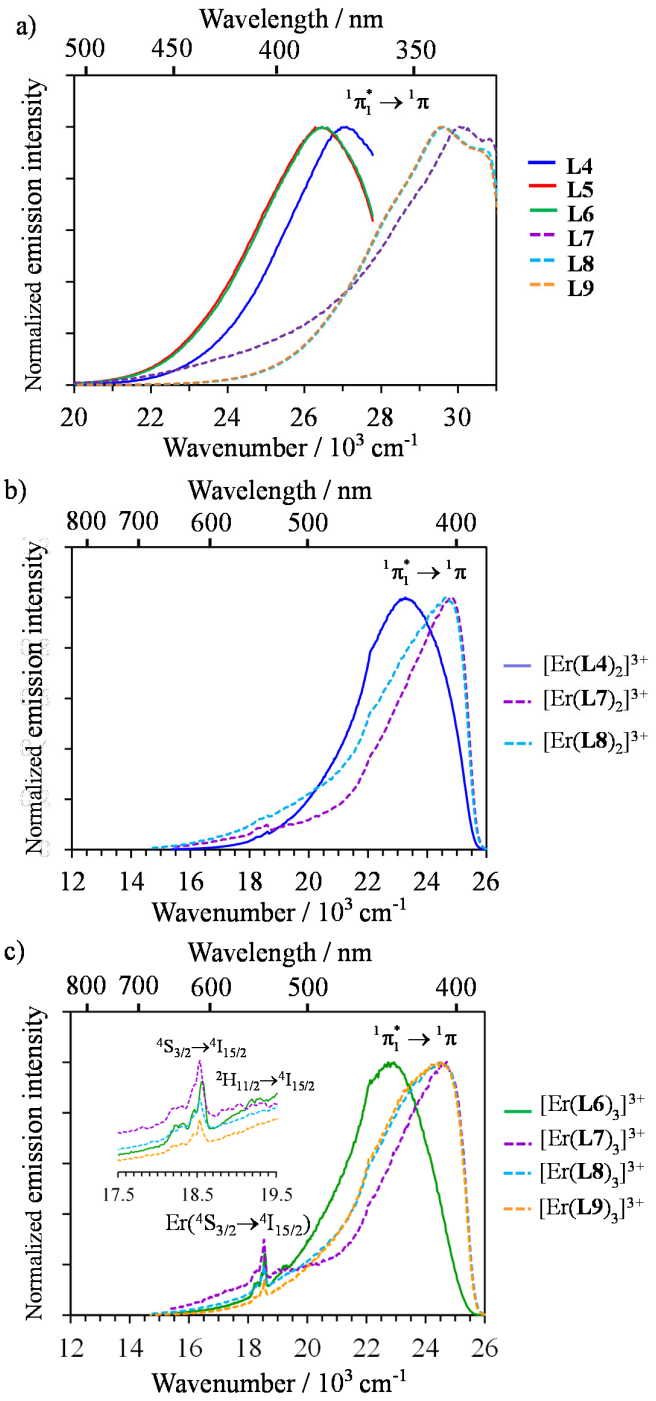

Figure 9. Emission spectra of a) ligands **L4-L6** (0.3 mM, λ_{exc} = 330 nm) and **L7-L9** (0.3 mM, λ_{exc} = 280 nm), b) 1:2 complexes **1-3** (3.0 mM) and c) 1:3 complexes **4-7** (3.0 mM) in acetonitrile solution at 298 K (λ_{exc} = 370 nm for complexes with **L4-L6** and λ_{exc} = 340 nm for complexes with **L7-L9**; a cutoff filter at 400 nm is used).

The electronic absorption spectra of the free ligands **L4-L9** in acetonitrile solution display the typical $\pi_1^* \leftarrow \pi$ transitions characteristic for the bisbzimpy (**L4**)[30],[60] and terpyridine (**L7**)[61] series (Figure

8a). The 4500 cm^{-1} red-shift combined with the doubling of the absorption coefficient resulting from the aromatic extension in going from the terpy series (**L7**-**L9**, dotted traces in Figure 8) to bisbzimpy (**L4**-**L6**, full traces in Figure 8) makes the latter ligands more efficient for acting as sensitizers for luminescent lanthanides in $[Ln(\mathbf{L}\boldsymbol{k})_n]^{3+}$ complexes.[62] The minor additional 400 cm^{-1} red-shift induced by the connection of methyl (**L5** and **L8**) or ethyl (**L6** and **L9**) groups to the distal aromatic rings are in line with the reduction of the HOMO-LUMO gap predicted by Extended Hückel Molecular Orbital calculations.[30] These global shifts toward lower energies are mirrored by similar trends observed in the associated emission spectra recorded in acetonitrile (298 K) upon excitation into the $\pi_1^* \leftarrow \pi$ transitions (Figure 9a). According to their nanosecond lifetimes (Table S38 and Figure S39), these emission bands can be safely assigned to singlet $^1\pi_1^* \rightarrow {}^1\pi$ transitions, the intensity of which can be magnified at lower temperature (77 K in frozen solution, Figure S40a) where the appearance of low-energy weak bands possessing longer lifetimes (> 1 μs, Figure S40b) can be attributed to the contribution of weak spin-forbidden $^3\pi_1^* \rightarrow {}^1\pi$ transitions. Upon complexation to Er^{3+} in $[Er(\mathbf{L}\boldsymbol{k})_n]^{3+}$ (n = 2, 3) at 3.0 mM concentration (> 90% of the ligand speciation corresponds to the target complex), the $\pi_1^* \leftarrow \pi$ transition undergoes the well-known $\pi_{1a},\pi_{1b}^* \leftarrow \pi$ splitting accompanying the *trans-trans* → *cis-cis* rearrangement of the aromatic tridentate ligand binding units: a spectral feature diagnostic for their meridional tri-coordination to a central metallic center (Figures 8b-c).[30],[60],[61] Concomitant measurements in the solid state (*i.e.* at higher concentration) confirm the latter splitting process (Figure S41) together with the detection of additional weak $Er(^{2S+1}L_J \leftarrow {}^4I_{15/2})$ absorption transitions covering the 6000-25000 cm^{-1} spectral window (Figure S42). Interestingly, the radiative lifetime associated to any emission transition terminating onto the ground $Er(^4I_{15/2})$ level can be estimated by its oscillator strength calculated with Eq. (12) where $\int \varepsilon(\tilde{\nu})\mathrm{d}\tilde{\nu}$ is the integrated spectrum of the incriminated absorption transition recorded in solution, J and J' refer to the ground (J = 15/2) and excited states, respectively, n is the refractive index of the medium, N_A is Avogadro's number, c is the speed of light in vacuum and $\tilde{\nu}_m$ is the barycenter of the transition (Table 2).[4]

$$\frac{1}{\tau_{rad}} = 2303 \cdot \frac{8\pi c n^2 \tilde{\nu}_m^{\ 2}(2J+1)}{N_A(2J'+1)} \int \varepsilon(\tilde{\nu}) d\tilde{\nu} \qquad (12)$$

Table 2 Radiative lifetimes calculated with Eq. (20) for selected Er(III) excited levels in the complexes **1**-**7** (acetonitrile, 298 K).

Compound	State / Solvent	$\tau_{Er,rad}^{4I_{13/2}}$ / ms	$\tau_{Er,rad}^{4I_{11/2}}$ / ms	$\tau_{Er,rad}^{4S_{3/2}}$ / μs	$\tau_{Er,rad}^{2H_{11/2}}$ / μs	$\tau_{Er,rad}^{4F_{7/2}}$ / μs
[Er(**L4**)$_2$(O_3SCF_3)$_2$](CF_3SO_3)	Solid[a]	6.3	4.3	546	177	246
	CH_3CN[b]	9.1	6.1	785	254	353
[Er(**L7**)$_2$(O_3SCF_3)$_2$](CF_3SO_3)	Solid[a]	6.1	5.6	515	301	269
	CH_3CN[b]	8.7	8.1	741	433	387
Er(**L8**)$_2$(O_3SCF_3)$_3$	Solid[a]	5.6	6.3	453	259	266
	CH_3CN[b]	8.0	9.0	651	372	382
[Er(**L6**)$_3$](ClO_4)$_3$	Solid[a]	6.3	5.4	716	282	405
	CH_3CN[b]	9.1	7.8	1029	406	582
[Er(**L7**)$_3$](ClO_4)$_3$	Solid[a]	6.4	4.4	476	442	352
	CH_3CN[b]	9.2	6.3	684	636	506
[Er(**L8**)$_3$](ClO_4)$_3$	Solid[a]	6.1	6.8	493	418	299
	CH_3CN[b]	8.8	9.8	709	602	430
[Er(**L9**)$_3$](ClO_4)$_3$	Solid[a]	6.1	6.9	495	435	299
	CH_3CN[b]	8.7	9.9	712	626	430

[a] For the solid-state samples, $\tau_{Er,rad}$ was calculated assuming that the structures are similar in different media and taking into account a simple n^3 dependence (Eq. (2)) of the refractive index with n_{solid} = 1.517 and n_{CH3CN} = 1.344.[4b],[63] [b] c = 3 mM.

Excitation into the ligand-centered **L*k***($\pi_{1b}^* \leftarrow \pi$) transition in the unsaturated [Er(**L*k***)$_2$]$^{3+}$ complexes (**L*k*** = **L4**, **L7**, **L8**) in solution at room temperature shows the residual emission of the ligand-centered singlet emission (Figure 9b and Table S39). Upon freezing the solution at 77 K, additional very weak

green Er($^4S_{3/2}\rightarrow{}^4I_{15/2}$) emission bands ($\tau(^4S_{3/2})$ = 8-12 ns, Table S40) can be identified around 18450 cm^{-1} (Figure S43), the intensity of which further increases for solid-state samples measured at 7-11 K (Figure S44). Compared with natural radiative lifetimes of $540 < \tau_{Er,rad}^{^4S_{3/2}} < 750$ µs calculated for this transition in the corresponding 1:2 complexes (Table 2, column 5), the observed nanosecond Er($^4S_{3/2}\rightarrow{}^4I_{15/2}$) emission corresponds to small Er-centered quantum yields $Q_{Er}^{Er}\left(^4S_{3/2}\right) = \tau_{Er,exp}^{^4S_{3/2}} / \tau_{Er,rad}^{^4S_{3/2}}$ < 0.002% (Table S40). The latter visible Er-centered luminescence becomes more sizeable in the saturated triple-stranded helical $[Er(\mathbf{L}\boldsymbol{k})_3]^{3+}$ complexes (**L*k*** = **L6**-**L9**), where it can be now easily detected at room temperature in solution (Figure 9c) additionally to the residual ligand-centered singlet emission (Table S41). This observation mirrors the previous and rather surprising report of detectable upconverted green Er($^4S_{3/2}\rightarrow{}^4I_{15/2}$) emission implemented in $[CrErCr(\mathbf{L1})_3]^{9+}$, a coordination complex possessing high-energy oscillators.[23a] Taking $\tau_{Er,exp}^{^4S_{3/2}}$ = 40(2) ns measured in $[GaErGa(\mathbf{L1})_3](CF_3SO_3)_9$ at 3K[23c] as an upper limit of the experimental Er($^4S_{3/2}$) lifetimes in these $[ErN_9]$ chromophores, the intrinsic quantum yield of the Er($^4S_{3/2}\rightarrow{}^4I_{15/2}$) emission still remains limited ($Q_{Er}^{Er}\left(^4S_{3/2}\right) < 0.01\%$) in mononuclear triple-helical complexes, but still roughly one order of magnitude larger than in unsaturated complexes. This observation justifies the use of solid-state samples of $[Er(\mathbf{L}\boldsymbol{k})_3](ClO_4)_3$ complexes (**L*k*** = **L6**-**L9**), where local concentration and antenna effect are maximized, for getting well-resolved emission spectra both at room temperature (Figure 10) and at 77 K (Figure S45). Beyond the uncommon visible Er($^4S_{3/2}\rightarrow{}^4I_{15/2}$) luminescence observed upon ligand-centered excitation (main plot in Figure 10), the latter triple helical complexes additionally display standard Er-centered infrared emission associated with Er($^4I_{13/2}\rightarrow{}^4I_{15/2}$) transitions occurring around 6300 cm^{-1} (inset in Figure 10), the room temperature lifetimes of which $1 < \tau_{Er,exp}^{^4I_{13/2}} < 6$ µs corresponds to intrinsic $Q_{Er}^{Er}\left(^4I_{15/2}\right) \approx 0.1\%$ quantum yields for the best protected $[Er(\mathbf{L6})_3](ClO_4)_3$ triple helix. It is worth noting here that the induction of dual Er-centered $^4S_{3/2}\rightarrow{}^4I_{15/2}$ (Visible) and $^4I_{13/2}\rightarrow{}^4I_{15/2}$ (NIR) emission is exceptional in coordination complexes and the detailed investigation

of the less-protected hydroxyl-bridged analogous $[(\mathbf{L4})_2Er(OH)_2Er(\mathbf{L4})_2](ClO_4)_4$ (**8**) and $[(\mathbf{L5})_2Er(OH)_2Er(\mathbf{L5})_2](ClO_4)_4$ (**9**), or solvent-bridged $[(\mathbf{L4})_2Er(CH_3NO_2)_2Er(\mathbf{L4})_2](ClO_4)_6$ (**10**) dimers indeed show no trace of visible emission, even in the solid state even at low temperature (Figure S46).

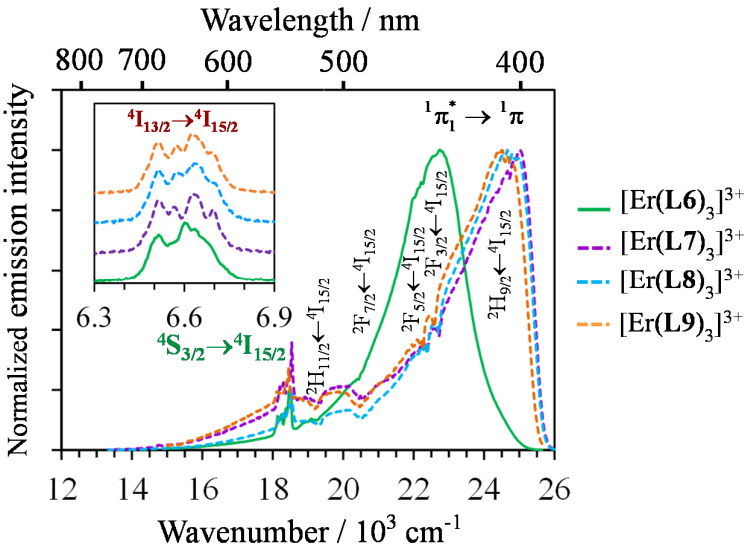

Figure 10. Dual visible (main plot) and near-infrared (inset) emission spectra recorded for the complexes **4** (λ_{exc} = 370 nm) and **5**-**7** (λ_{exc} = 340 nm) in the solid-state at room temperature. The dual emission is assigned using color fonts, while the dips (assigned using black fonts) correspond to Er-centered re-absorption of the residual ligand-centered $^1\pi^*\rightarrow\pi$ emission.

Conclusion

In our attempt to reproduce the intriguing luminescent properties of $[ErN_9]$ chromophores found in the self-assembled trinuclear d-f helicate $[CrErCr(\mathbf{L1})_3]^{9+}$ (Scheme 2), into simple, stable and tunable mononuclear triple-helical model complexes $[Er(\mathbf{L}\boldsymbol{k})_3]^{3+}$ ($\mathbf{L}\boldsymbol{k}$ = **L4**-**L9**), we discovered that the stereo-electronic requirements responsible for the uncommon room-temperature dual Er-centered visible/near-infrared emission essentially depend on the tight wrapping of the three polyaromatic strands around the metallic center. The Jablonski diagram shown in Figure 11 summarizes the established mechanisms responsible for the generation of the dual visible/near-infrared luminescence in the triple helical $[Er(\mathbf{L}\boldsymbol{k})_3]^{3+}$ complexes ($\mathbf{L}\boldsymbol{k}$ = **L6**-**L9**).

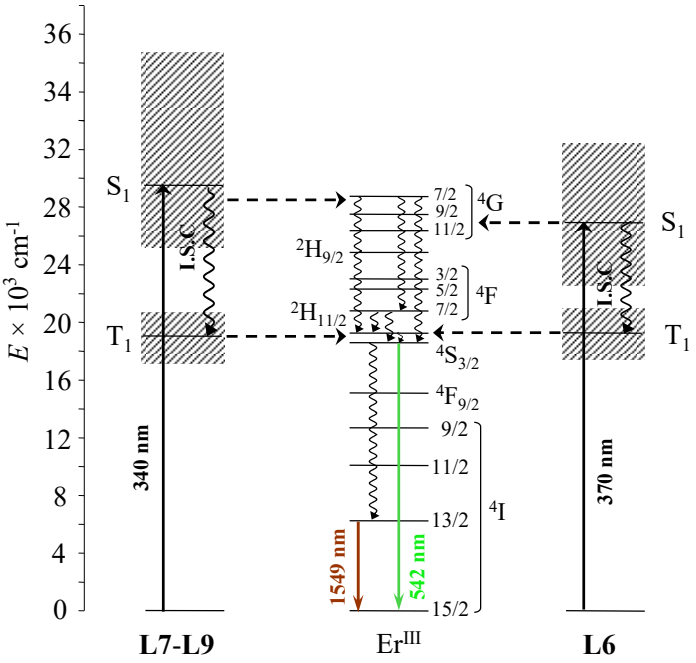

Figure 11. Jablonski diagram summarizing the excitation processes (straight upward arrows), energy transfers (dashed arrows), non-radiative multiphonon relaxation (undulating arrows) and radiative emission processes (straight downward arrows) operating in the triple-helical complexes $[Er(\mathbf{L}\boldsymbol{k})_3]^{3+}$ (**L*k*** = **6**-**9**). Ligand-to-metal energy transfers arising from both singlet and triplet states are considered.

The replacement of one ligand strand with low-frequency oscillators triflate counter-anions in $[Er(\mathbf{L}\boldsymbol{k})_2(CF_3SO_3)_n]^{(3-n)+}$ chromophores (n = 2, 3) is still compatible with the detection of very weak green $Er(^4S_{3/2} \rightarrow {}^4I_{15/2})$ emission at 542 nm, but only at low temperature. As soon as hydroxide anions (OH oscillators) or solvent molecules (CH oscillators) are bound in the Er(III) first coordination sphere in the dimers $[(\mathbf{L4})_2Er(OH)_2Er(\mathbf{L4})_2](ClO_4)_4$ (**8**), $[(\mathbf{L5})_2Er(OH)_2Er(\mathbf{L5})_2](ClO_4)_4$ (**9**) and $[(\mathbf{L4})_2Er(CH_3NO_2)_2Er(\mathbf{L4})_2](ClO_4)_6$ (**10**), the visible emission is totally quenched. The extension of the aromatic units in going from the terpy series (**L7**-**L9**, Scheme 4) to the bisbzimpy series (**L4**-**L6**, Scheme 3) shifts the ligand-centered absorption bands toward lower energies, a trend in line with potential visible sensitization of Er-centered luminescence in $[Er(\mathbf{L4})_3]^{3+}$, a process which is not accessible for $[Er(\mathbf{L7})_3]^{3+}$. A further red-shift accompanies the peripheral substitution with terminal methyl (**L5**, **L8**) or ethyl (**L6**, **L9**) groups, but no spectacular luminescence change results from the protection of the termini of the $[Er(\mathbf{L}\boldsymbol{k})_3]^{3+}$ triple-helix with these ligands. However, the systematic

(often tedious) preparation and analysis of the H→methyl→ethyl structural series demonstrates its pertinence for the rationalization of (i) the driving forces controlling the intermolecular interactions operating in the solid state, which are responsible for phase transition temperatures, and (ii) the solvation energies pertinent to thermodynamic association processes occurring in solution. To summarize, we are now fully equipped for the molecular design of stable erbium coordination complexes, the ErN_9 chromophore of which displays room temperature dual visible/near-infrared emission in solution and in the solid state at room temperature. Further use as activators for molecular-based excited state absorption (ESA) and energy-transfer (ETU) linear upconversion are currently under investigation.

Acknowledgements

Financial support from the Swiss National Science Foundation is gratefully acknowledged. The work performed in France was supported by La Ligue contre le Cancer, Cancéropôle Grand Ouest, Agence Nationale de la Recherche (ANR-13-BS08-0011) and INSERM.

Conflicts of interest

The authors declare no conflict of interest

Keywords: erbium complexes, thermodynamics, dual emission, solvation, triple helical

References

[1] a) C. Piguet, *Nature Chemistry* **2014**, *6*, 370; b) C.-G. Ma, M. G. Brik, D.-X. Liu, B. Feng, Y. Tian, A. Suchocki, *J. Luminesc.* **2016**, *170*, 369-374.

[2] a) A. Einstein, *Phys. Z.* **1917**, *18*, 121–128; b) S. Strickler, S. J. Berg, *J. Chem. Phys.* **1962**, *37*, 814–822; c) J. B. Berks, D. J. Dyson, *R. London Soc. Ser. A* **1963**, *275*, 135–148.

[3] a) W. T. Carnall, *Handbook on the Physics and Chemistry of Rare Earths*, K. A. Gschneidner and L. Eyring, Eds. North-Holland Publishing Company: Amsterdam, New York, Oxford, 1979; Vol. 3, chap 24, pp 171-208; b) J.-C. G. Bünzli, S. V. Eliseeva, *Lanthanide*

Luminescence: Photophysical, Analytical and Biological Aspects, P. Hänninen and H. Härmä, H., Eds. Springer-Verlag: Berlin Heidelberg, 2010; Vol. 7, pp 1-45.

[4] a) L. D. Carlos, R. A. S. Ferreira, V. D. Bermudez, S. J. L. Ribeiro, *Adv. Mater.* **2009**, *21*, 509-534; b) J.-C. G. Bünzli, A.-S. Chauvin, H. K. Kim, E. Deiters, S. V. Eliseeva, *Coord. Chem. Rev.* **2010**, *254*, 2623-2633.

[5] T. C. Brunold, H. U. Güdel, *Inorganic Electronic Structures and Spectroscopy*; E. I. Solomon and A. B. P. Lever, Eds; Wiley: New York, 1999, pp 259-306.

[6] C. Reinhard, H. U. Güdel, *Inorg. Chem.* **2002**, *41*, 1048-1055.

[7] F. Artizzu, M. L. Mercuri, A. Serpe, P. Deplano, *Coord. Chem. Rev.* **2011**, *255*, 2514-2529.

[8] D. K. Sardar, S. Chandrasekharan, K. L. Nash, J. B. Gruber, *J. Appl. Phys.* **2008**, *104*, 023102.

[9] T. Feuchter, E. K. Mwarania, J. Wang, L. Reekie, J. S. Williams, *IEEE Photonics Technol. Lett.* **1992**, *4*, 542-544.

[10] G. N. van den Hoven, R. J. I. M. Koper, A. Polman, C. van Dam, J. W. M. Uffelen, K. M. Smit, *Appl. Phys. Lett.* **1996**, *68*, 1886-1888.

[11] P. Becker, R. Brinkmann, M. Dinand, W. Sohler, H. Suche, *Appl. Phys. Lett.* **1992**, *61*, 1257-1259.

[12] K. Kuriki, K. Koike, Y. Okamoto, *Chem. Rev.* **2002**, *102*, 2347-2356.

[13] a) J. Kido, Y. Okamoto, *Chem. Rev.* **2002**, *102*, 2357-2368; b) P. Martin-Ramos, C. Coya, A. L. Alvarez, M. Ramos Silva, C. Zaldo, J. A. Paixao, P. Chamorro-Posada, J. Martin-Gil, *J. Phys. Chem. C* **2013**, *117*, 10020-10030; c) H. Wei, G. Yu, Z. Zhao, Z. Liu, Z. Bian, C. Huang, *Dalton Trans.* **2013**, *42*, 8951-8960.

[14] a) J. W. Hofstraat, M. P. Oude Wolbers, F. C. J. M. Van Veggel, D. Reinhoudt, M. H. V. Werts, J. W. Verhoeven, *J. Fluoresc.* **1998**, *8*, 301-308; b) S. Quici, G. Marzanni, A. Forni, G. Accorsi, F. Barigelletti, *Inorg. Chem.* **2004**, *43*, 1294-1301; c) G. M. Davies, H. Adams, S. J. A. Pope, S. Faulkner, M. D. Ward, *Photochem. Photobiol. Sci.* **2005**, *4*, 829-834; d) S. Comby, D. Imbert, C. Vandevyver, J.-C. G. Bünzli, *Chem. Eur. J.* **2007**, *13*, 936-944.

[15] a) A. Mech, A. Monguzzi, F. Meinardi, J. Mezyk, G. Macchi, R. Tubino, *J. Am. Chem. Soc.* **2010**, *132*, 4574-4576; b) E. R. Triveldi, S. V. Eliseeva, J. Jankolovits, M. M. Olmstead, S. Petoud, V. L. Pecoraro, *J. Am. Chem. Soc.* **2014**, *136*, 1526-1534; c) B. L. Reid, S. Stagni, J. M. Malicka, M. Cocchi, A. N. Sobolev, B. W. Skelton, E. G. Moore, G. S. Hanan, M. I. Ogden, M. Massi, *Chem. Eur. J.* **2015**, *21*, 18354-18363; d) Y. Peng, J. X. Xu, H. Lu, R. M. Wilson, M. Motevalli, I. Hernandez, W. P. Gillin, P. B. Wyatt, H. Q. Ye, *RSC Adv.* **2017**, *7*, 128-131.

[16] a) G. Mancino, A. J. Ferguson, A Beeby, N. J. Long, T. S. Jones, *J. Am. Chem. Soc.* **2005**, *127*, 524-5251; b) P. B. Glover, A. P. Basset, P. Nockemann, B. M. Kariuki, R. Van Deun, Z. Pikramenou, *Chem. Eur. J.* **2007**, *13*, 6309-6320; c) L. Song, J. Hu, J. Wang, X. Liu, Z. Zhen, *Photochem. Photobiol. Sci.* **2008**, *7*, 689-693; d) C. Doffek, N., Alzakhem, M. Molon, M. Seitz, *Inorg. Chem.* **2012**, *51*, 4539-4545.

[17] a) F. Auzel, *Chem. Rev.* **2004**, *104*, 139-173; b) B. M. van der Ende, L. Aarts, A. Meijerink, *Phys. Chem. Chem. Phys.* **2009**, *11*, 11081-11095.

[18] N. Bloembergen, *Phys. Rev. Lett.* **1959**, *2*, 84-85,

[19] a) F. Auzel, *C. R. Acad. Sc. Paris* **1966**, *B262*, 1016-1019; b) F. Auzel, *C. R. Acad. Sc. Paris* **1966**, *B263*, 819-821.

[20] a) G. Chem, H. Qiu, P. N. Prasad, X. Chen, *Chem. Rev.* **2014**, *114*, 5161-5214; b) P. Ramasamy, P. Manivasakan, J. Y. Kim, *RSC Adv.* **2014**, *4*, 34873-34895; c) J. Zhou, Q. Liu, W. Feng, Y. Sun, F. Li, *Chem. Rev.* **2015**, *115*, 395-465; d) S. Ye, E.-H. Song, Q.-Y. Zhang, *Adv. Sci.* **2016**, *3*, 1600302; e) R. Medishetty, J. K. Zareba, D. Mayer, M. Samoc, R. A. Fischer, *Chem. Soc. Rev.* **2017**, *46*, 4976-5004; f) X.-Y. Wang, R. R. Valiev, T. Y. Ohulchanskyy, H. Agren, C. Yang, G. Chen, *Chem. Soc. Rev.* **2017**, *46*, 4150-4167.

[21] a) Y. Suffren, B. Golesorkhi, D. Zare, L. Guénée, H. Nozary, S. V. Eliseeva, S Petoud, A. Hauser, C. Piguet, *Inorg. Chem.* **2016**, *55*, 9964-9972; b) L. J. Charbonnière, *Dalton Trans.*, 2018 DOI 10.1039/c7dt04737a.

[22] I. Hyppänen, S. Lahtinen, T. Ääritalo, J. Mäkelä, J. Kankare, T. Soukka, *ACS Photonics* **2014**, *1*, 394-397.

[23] a) L. Aboshyan-Sorgho, C. Besnard, P. Pattison, K. R. Kittilstved, A. Aebischer, J.-C. G. Bünzli, A. Hauser, C. Piguet, *Angew. Chem. Int. Ed.* **2011**, *50*, 4108-4112; b) Y. Suffren, D. Zare, S. V. Eliseeva, L. Guénée, H. Nozary, T. Lathion, L. Aboshyan-Sorgho, S. Petoud, A. Hauser, C. Piguet, *J. Phys. Chem. C* **2013**, *117*, 26957-26963; c) D. Zare, Y. Suffren, L. Guénée, S. V. Eliseeva, H. Nozary, L. Aboshyan-Sorgho, S. Petoud, A. Hauser, C. Piguet, *Dalton Trans.* **2015**, *44*, 2529-2540.

[24] A. Nonat, C.F. Chan, C. Platas-Iglesias, Z. Liu, W.-T. Wong, W.-K. Wong, K.-L. Wong, L. J. Charbonnière, *Nature Commun.* **2016**, 11978.

[25] T. V. Balashova, A. P. Pushkarev, A. N. Yablonskiy, B. A. Andreev, I. D. Grishin, R. V. Rumyantcev, G. K. Fukin, M. N. Bochkarev, *J. Luminesc.* **2017**, *192*, 208-210.

[26] M. Haase, H. Schäfer, *Angew. Chem. Int. Ed.* **2011**, *50*, 5808-5829.

[27] a) M. T. Berry, P. S. May, *J. Phys. Chem. A* **2015**, *119*, 9805-9811; b) X. Shang, P. Chen, T. Jia, D. Feng, S. Zhang, Z.-M. Sun, J. Qiu, *Phys. Chem. Chem. Phys.* **2015**, *17*, 11481-11489; c) I. Hyppänen, N. Hoÿsniemi, R. Arppe, M. Schäferling, T. Soukka, *J. Phys. Chem. C* **2017**, *121*, 6924-6929.

[28] C. Piguet, J.-C. G. Bünzli, G. Bernardinelli, A. F. Williams, *Inorg. Chem.* **1993**, *32*, 4139-4149.

[29] G. Muller, J.-C. G. Bünzli, K. J. Schenk, C. Piguet, G. Hopfgartner, *Inorg. Chem.* **2001**, *40*, 2642-2651.

[30] C. Piguet, J.-C. G. Bünzli, G. Bernardinelli, C. G. Bochet, P. Froidevaux, *J. Chem. Soc.*, *Dalton Trans.* **1995**, 83-97.

[31] S. Petoud, J.-C. G. Bünzli, F. Renaud, C. Piguet, K. J. Schenk, G. Hopfgartner, *Inorg. Chem.* **1997**, *36*, 5750-5760.

[32] a) C. Piguet, B. Bocquet, G. Hopfgartner, *Helv. Chim. Acta* **1994**, *77*, 931-942; b) B. M. McKenzie, A. K. Miller, R. J. Wojtecki, J. C. Johnson, K. A. Burke, K. A. Tzeng, P. T. Mather S. J. Rowan, *Tetrahedron* **2008**, *64*, 8488-8495.

[33] L. F. Silva, M. V. Craveiro, *Org. Lett.* **2008**, *10*, 5417-5420.

[34] a) R. D. Chapman, R. T. Loda, J. P. Riehl, R. W. Schwartz, *Inorg. Chem.* **1984**, *23*, 1652-1657; b) L. I. Semenova, A. N. Sobolev, B. W. Skelton, A. H. White, *Aust. J. Chem.* **1999**, *52*, 519-529; c) M. G. B. Drew, P. B. Iveson, M. J. Hudson, J. O. Liljenzin, L. Spjuth, P.-Y. Cordier, A. Enarsson, C. Hill, C.; Madic, *J. Chem. Soc., Dalton Trans.* **2000**, 821-830; d) M. G. B. Drew, M. J. Hudson, P. B. Iveson, C. Madic, M. L. Russel, *J. Chem. Soc., Dalton Trans.* **2000**, 2711-2720; e) H.-R. Mürner, E. Chassat, R. P. Thummel, J.-C. G. Bünzli, *J. Chem. Soc., Dalton Trans.* **2000**, 2809-2816; f) L. Petit, C. Daul, C. Adamo, P. Maldivi, *New J. Chem.* **2007**, *31*, 1738-1745; g) J. M. Hamilton, M. J. Anhorn, K. A. Oscarson, J. H. Reibenspies, R. D. Hancock, *Inorg. Chem.* **2011**, *50*, 2764-2770.

[35] A. Fürstner, A. Leitner, M. Mendez, H. Krause, *J. Am. Chem. Soc.* **2002**, *124*, 13856-13863.

[36] R.-A. Fallahpour, M. Neuburger, M. Zehnder, *New J. Chem.* **1999**, 53-61.

[37] C. Bolm, M. Ewald, M. Felder, G. Schlingloff, *Chem. Ber.* **1992**, *125*, 1169-1190.

[38] J. Mathieu, P. Gros, Y. Fort, *Chem. Commun.* **2000**, 951-952.

[39] J.-M. Bénech, C. Piguet, G. Bernardinelli, J.-C. G.; Bünzli, G.; Hopfgartner, *J. Chem. Soc., Dalton Trans.* **2001**, 684-689.

[40] C. A. Bessel, R. F. See, D. L. Jameson, M. R. Churchill, K. J. Takeuchi, *J. Chem. Soc., Dalton Trans.* **1992**, 3223-3228.

[41] a) D. M. Ford, *J. Am. Chem. Soc.* **2005**, *127*, 16167-16170; b) O. A. Khakhel', *Chem. Phys. Lett.* **2006**, *421*, 464-468; c) O. A. Khakhel', T. P. Romashko, Y. E. Sakhno, *J. Phys. Chem. B.* **2007**, *111*, 7331-7335; d) C. Piguet, *Dalton Trans.* 2011, **40**, 8059-8071; e) O. A. Khakhel', T. P. Romashko, *J. Phys. Chem. A.* **2016**, *120*, 2035-2040.

[42] a) T. Dutronc, E. Terazzi, L. Guénée, K.-L. Buchwalder, A. Spoerri, D. Emery, J. Mareda, S. Floquet, C. Piguet, *Chem. Eur. J.* **2013**, *19*, 8447-8456; b) T. Dutronc, E. Terazzi, L. Guénée,

K.-L. Buchwalder, S. Floquet, C. Piguet, *Chem. Eur. J.* **2016**, *22*, 1385-1391; c) S. Guerra, T. Dutronc, E. Terazzi, L. Guénée, C. Piguet, *Phys. Chem. Chem. Phys.* **2016**, *18*, 14479-14494.

[43] a) C. Piguet, G. Hopfgartner, J. D. Henion, A. F. Williams, *Helv. Chim. Acta* **1993**, *76*, 1759-1766; b) R. Colton, A. D'Agostino, J. C. Traeger, *Mass Spectrom. Rev.* **1995**, *14*, 79-106; c) E. Leize, A. Jaffrezic, A. van Dorsselaer, *J. Mass Spectrom.* **1996**, *31*, 537-544.

[44] B. M. Castellano, D. K. Eggers, *J. Phys. Chem. B* **2013**, *117*, 8180-8188.

[45] b) K. Baudet, S. Guerra, C. Piguet, *Chem. Eur. J.* **2017**, *23*, 16787-16798.

[46] N. Ouali, B. Bocquet, S. Rigault, P.-Y. Morgantini, J. Weber, C. Piguet, *Inorg. Chem.* **2002**, *41*, 1436-1445.

[47] M. Pons, O. Millet, *Prog. Nucl. Magn. Reson. Spec.* **2001**, *38*, 267-324.

[48] a) E. R. Malinowski, D. G. Howery, *Factor Analysis in Chemistry*, Wiley, New York, Chichester, 1980; b) H. Gampp, M. Maeder, C. J. Meyer, A. Zuberbühler, *Talanta* **1986**, *33*, 943-951; c) B. R. Hall, L. E. Manck, I. S. Tidmarsh, A. Stephenson, B. F. Taylor, E. J. Blaikie, D. A. Vander Griend, M. D. Ward, *Dalton Trans.* **2011**, *40*, 12132-12145.

[49] a) H. Gampp, M. Maeder, C. J. Meyer, A. Zuberbühler, *Talanta* **1985**, *32*, 1133-1139; b) M. Maeder, P. King, *Analysis of Chemical Processes, Determination of the Reaction Mechanism and Fitting of Equilibrium and Rate Constants*, in Chemometrics in Practical Applications, Dr. Kurt Varmuza (Ed.), ISBN: 978-953-51-0438-4, InTech, DOI: 10.5772/31896; c) Specfit/32 from ReactLab Equilibria : http://jplusconsulting.com/products/reactlab-equilibria/.

[50] J.-C. G. Bünzli, A. E. Merbach, R. M. Nielson, *Inorg. Chim. Acta* **1987**, *139*, 151-152.

[51] G. Bodizs, I. Raabe, R. Scopelliti, I. Krossing, L. Helm, *Dalton Trans.* **2009**, 5137-5147.

[52] a) M. Borkovec, G. J. M. Koper, *J. Phys. Chem. B* **1994**, *98*, 6038-6045; b) G. J. M. Koper, M. Borkovec, *J. Phys. Chem. B* **2001**, *105*, 6666-6674; c) M. Borkovec, G. J. M. Koper, C. Piguet, *Curr. Opinion in Coll. and Int. Science* **2006**, *11*, 280-289; d) G. J. M. Koper, M. Borkovec, *Polymer* **2010**, *51*, 5649-5662; e) C. Piguet, *Chem. Commun.* **2010**, *46*, 6209-6231.

[53] a) S. W. Benson, *J. Am. Chem. Soc.* **1958**, *80*, 5151-5154; b) G. Ercolani, C. Piguet, M. Borkovec, J. Hamacek, *J. Phys. Chem. B* **2007**, *111*, 12195-12203.

[54] G. Ercolani, L. Schiaffino, *Angew. Chem. Int. Ed.* **2011**, *50*, 1762-1768.

[55] The molecular volumes are taken as the Connolly volumes, which are obtained from the building of the Connolly surface around the molecular structures of complexes observed in their crystal structure and by using a probe radius of 1.4 Å for modelling water solvent molecule. a) M. L. Connolly, *Science* **1983**, *221*, 709-713; b) M. L. Connolly, *J. Appl. Cryst.* **1983**, *16*, 548-558.

[56] T. Riis-Johannessen, N. Dalla Favera, T. K. Todorova, S. M. Huber, L. Gagliardi, C. Piguet, *Chem. Eur. J.* **2009**, *15*, 12702-12718.

[57] L. Babel, L. Guénée, C. Besnard, S. V. Eliseeva, S. Petoud, C. Piguet, *Chem. Sci.* **2018**, *9*, 325-335.

[58] a) I. D. Brown, D. Altermatt, *Acta Cryst B* **1985**, *B41*, 244-247; b) N. E. Breese, M. O'Keeffe, *Acta Cryst. B* **1991**, *B47*, 192-197; c) I. D. Brown, *Acta Cryst B* **1992**, *B48*, 553-572; d) I. D. Brown, *The Chemical Bond in Inorganic Chemistry,* Oxford University Press, UK, 2002; e) A. Trzesowska, R. Kruszynski, T. J. Bartczak, *Acta Cryst B Structural Science* **2004**, *B60*, 174-178; f) A. Trzesowska, R. Kruszynski, T. J. Bartczak, *Acta Cryst B Structural Science* **2005**, *B61*, 429-434; g) A Trzesowska, R Kruszynski, T. J. Bartczak, *Acta Cryst B Structural Science* **2006**, *B62*, 745-753; h) F. Zocchi, *J. Mol. Struct. Theochem.* **2007**, *805*, 73-78; (*i*) I. D. Brown, *Chem. Rev.* **2009**, *109*, 6858-6919.

[59] a) C. A. Hunter, K. R. Lawson, J Perkins, C. J. Urch, *J. Chem. Soc., Perkin 2* **2001**, 651-669; b) S. Grimme, *Angew. Chem. Int. Ed.* **2008**, *47*, 3430-3434; c) K. E. Riley, P. Hobza, *Acc. Chem. Res.* **2013**, *46*, 927-936.

[60] a) C. Piguet, B. Bocquet, E. Müller, A. F. Williams, *Helv. Chim. Acta* **1989**, *72*, 323-337; b) E. Terazzi, L. Guénée, P.-Y. Morgantini, G. Bernardinelli, B. Donnio, D. Guillon, C. Piguet, *Chem. Eur. J.* **2007**, *13*, 1674-1691.

[61] a) K. Nakamoto, *J. Phys. Chem.* **1960**, *64*, 1420-1425; b) S. Xu, J. E. T. Smith, J. M. Weber, *Inorg. Chem.* **2016**, *55*, 11937-11943.

[62] C. Piguet, J.-C. G. Bünzli, *Handbook on the Physics and Chemistry of Rare Earths*, K. A. GschneidnerJr, J.-C. G. Bünzli, V. K. Pecharsky, Eds. Elsevier Science: Amsterdam, 2010; Vol. 40, pp 301-553.

[63] Z. Wang, T. Senden, A. Meijerink, *J. Phys. Chem. Lett.* **2017**, *8*, 5689-5694.

TOC

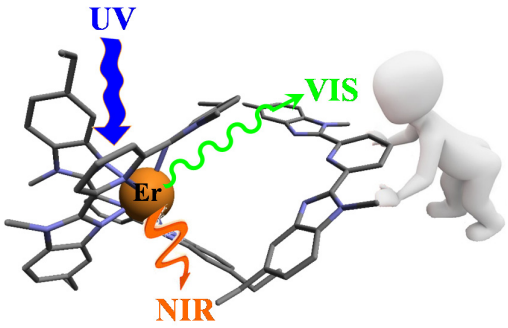

The thermodynamic assembly of three tridentate aromatic strands around trivalent erbium in triple-helical $[Er(\mathbf{L}\boldsymbol{k})_3]^{3+}$ complexes is the necessary condition for inducing some rare dual visible/near-infrared luminescence at room temperature in the solid state and in solution: a prerequisite for implementing lanthanide-based upconversion at the molecular level.